10

Functionalization of COFs

10.1 Introduction

In Chapters 7 through 9 we have outlined how the structure type, metrics, and type of linkage in covalent organic frameworks (COFs) can be tailored. These parameters dictate the physical properties of COFs such as their chemical and thermal stability, as well as crystallinity and porosity. To devise materials with specific function or to fine-tune the properties of a given COF for a targeted application, functionality needs to be introduced. This is achieved by the introduction of guest molecules in the pores of the COF, by covalent modification of the frameworks' backbone, and by metalation of specific binding sites within the structure. Historically, much of what has been reported in the functionalization of COFs was inspired by work on discrete molecules and the vast toolbox of synthetic organic and organometallic chemistry. The organic backbone of COFs can be functionalized both pre- and post-synthetically to introduce functional groups into specific positions within the framework. Similarly, pre- and post-synthetic metalation of frameworks at predesigned metal coordination sites can be achieved. Here, it is important to consider that applying this know-how to the solid state strictly requires a porous material. In the case of pre-synthetic modifications, the porous nature ensures the necessary space for the introduction of the functionality into the framework without affecting changes to the overall structure metrics or structure type. With respect to post-synthetic modification, porosity is required to guarantee the addressability of the framework constituents to the reagents. The functionalization of COFs exceeds what can be done in molecular chemistry because their porosity further enables additional modes of functionalization such as trapping of functional guests in the pores and embedding of molecular entities within the extended crystals of COFs.

10.2 *In situ* Modification

A simple way to introduce functionality into COFs is to embed large functional guests within their pores. This mode of functionalization is affected *in situ* during the COF synthesis because the introduced guests exceed the

Introduction to Reticular Chemistry: Metal-Organic Frameworks and Covalent Organic Frameworks,
First Edition. Omar M. Yaghi, Markus J. Kalmutzki, and Christian S. Diercks.

Companion website: www.wiley.com/go/yaghi/reticular

size of the pores (ship-in-a-bottle), which precludes post-synthetic introduction of these species into the framework. Theoretically, a large number of potential guests such as biomolecules, polyoxometallates, or metal nanoparticles can be introduced with this strategy but thus far the feasibility of this approach has only been demonstrated for the incorporation of metal-oxide nanoparticles.

10.2.1 Embedding Nanoparticles in COFs

The formation of nanoparticles embedded in COFs is difficult because the controlled precipitation of these materials from a homogeneous solution poses a significant challenge, an issue that will be covered in more detail in Chapter 11. One strategy to circumvent this is to coat the nanoparticles with an amorphous imine polymer of controllable thickness in a first step and to subsequently transform it to a crystalline COF in a second step (Figure 10.1a). $[(TFP)_2(BZ)_3]_{\beta\text{-}ketoenamine}$ is constructed from trigonal tritopic TFP and linear ditopic BZ (benzidine) building units (Figure 10.1b). Under conventional COF forming conditions and in the presence of an acid catalyst, $[(TFP)_2(BZ)_3]_{\beta\text{-}ketoenamine}$ precipitates from solution in an uncontrolled fashion [1]. To grow the COF around Fe_3O_4 nanoparticles they are therefore first coated with an amorphous imine polymer of the same composition to achieve control over the nucleation process. This is achieved in the absence of acid, and the imine polymer grows exclusively around the nanoparticles added to the solution. After isolation of the nanoparticles coated with a layer of amorphous imine polymer (Fe_3O_4⊂Polyimine) of controllable thickness the material is subjected to a solution containing 10% of the organic base pyrrolidine resulting in reversible error correction of the material and the formation of a crystalline $[(TFP)_2(BZ)_3]_{\beta\text{-}ketoenamine}$ shell around the nanoparticles (Fe_3O_4⊂$[(TFP)_2(BZ)_3]_{\beta\text{-}ketoenamine}$) (Figure 10.1b). This amorphous to crystalline transformation is not only corroborated by powder X-ray diffraction but also by a substantial improvement in the surface area of the respective materials. Fe_3O_4⊂$[(TFP)_2(BZ)_3]_{\beta\text{-}ketoenamine}$ has a surface area of 1346 $m^2\ g^{-1}$, whereas the amorphous Fe_3O_4⊂Polyimine has a surface area of 255 $m^2\ g^{-1}$, and the isolated nanoparticles have a surface area of just 123 $m^2\ g^{-1}$ [2].

The generality of the amorphous to crystalline transformation approach for the formation of NP⊂COF (NP = nanoparticle) core-shell structures is further supported by its applicability to imine-linked COFs such as $[(TAPB)(TFB)]_{imine}$, a material composed of trigonal tritopic TFB and trigonal tritopic TAPB building units (Figure 10.1c). Nanoparticles of various chemical nature and size can be incorporated: Fe_3O_4 (9.8 nm), Au (9.0 nm), and Pd (3.3 nm). Analogous to the case of the ketoenamine linked framework, the strategy for coating nanoparticles with $[(TAPB)(TFB)]_{imine}$ relies on the formation of an amorphous imine polymer to control the nucleation. In contrast, the subsequent crystallization step to yield the crystalline imine-linked COF is carried out in the presence of aqueous acetic acid [3].

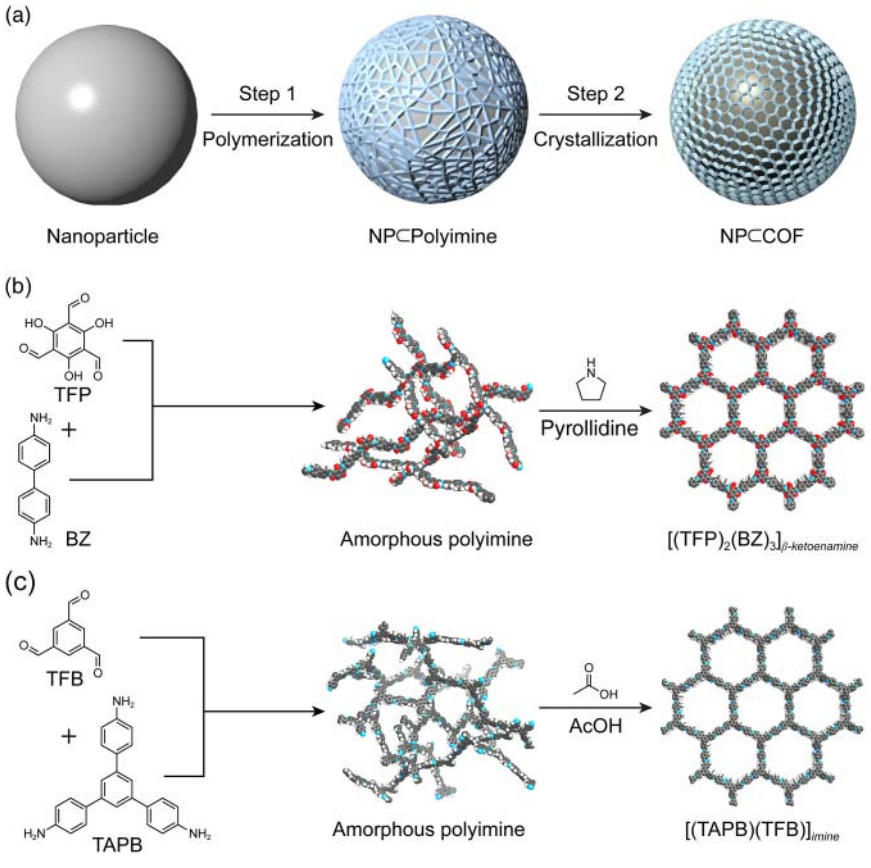

Figure 10.1 Formation of COF-coated nanoparticles in a two-step process (a). In the first step the nanoparticles (gray spheres) are coated by an amorphous imine polymer in the absence of a catalyst under homogeneous conditions, thus allowing for controlled nucleation. In a second step the polymer is converted into a crystalline COF through dynamic error correction in the presence of a catalyst. (b) Reaction of trigonal tritopic TFP with linear ditopic BZ in the absence of catalyst yields an amorphous imine polymer that can subsequently be converted into crystalline $[(TFP)_2(BZ)_3]_{\beta\text{-ketoenamine}}$ by exposing the material to a 10% solution of pyrollidine as a catalyst at elevated temperatures. (c) Reaction of TFB and TAPB yields an amorphous imine polymer. Exposing the polymer to a solution of acetic acid at elevated temperatures yields crystalline $[(TAPB)(TFB)]_{imine}$. Color code in (b) and (c): H, white; C, gray; N, blue; O, red.

10.3 Pre-Synthetic Modification

We have shown previously, that by choosing linkers of the same connectivity and geometry but with different metrics, isoreticular expansion of COFs is performed to adjust the pore metrics of a given framework. The isoreticular principle is not limited to adjusting the pore metrics but can furthermore be applied to the functionalization of frameworks, where metal ions are coordinated to, or functional groups appended onto specific sites of the linker without interfering with

the overall structure metrics of the resulting COF. If the appended functionality does not interfere with the COF forming reaction these modifications can be affected pre-synthetically, which enables the formation of the functionalized framework in one step. Pre-synthetic modification of building units is the most common approach for the functionalization of COFs, and many different of functional groups can be incorporated according to this strategy. A large number of examples of pre-synthetic modification will be highlighted throughout this chapter as this type of functionalization also forms the basis for subsequent post-synthetic modifications. Consequently, we restrict this section to highlighting the versatility of this concept using illustrative examples that convey the general underlying concepts of and motivation for pre-synthetic modification.

10.3.1 Pre-Synthetic Metalation

The imine-linked COF-366 shows promise with respect to applications in organic electronics owing to its inherent high charge carrier mobility of 8.1 $cm^2\ V^{-1}\ s^{-1}$ [4]. COF-366 is constructed from square planar tetratopic H_2TAP and linear ditopic BDA (terephthaldehyde) building units by imine bond formation, yielding a framework of **sql** topology. To introduce functionality into the structure the porphyrin core can serve as a metal coordination site. An isoreticular functionalized analog of the framework, termed COF-366-Co $[(Co(TAP))(BDA)_2]_{imine}$, is constructed from the metalated Co(TAP) (tetra(4-aminophenyl)porphinato cobalt) and BDA (Figure 10.2). The Co(TAP) building unit is stable to the COF forming reaction, allowing for its introduction during the synthesis. Cobalt

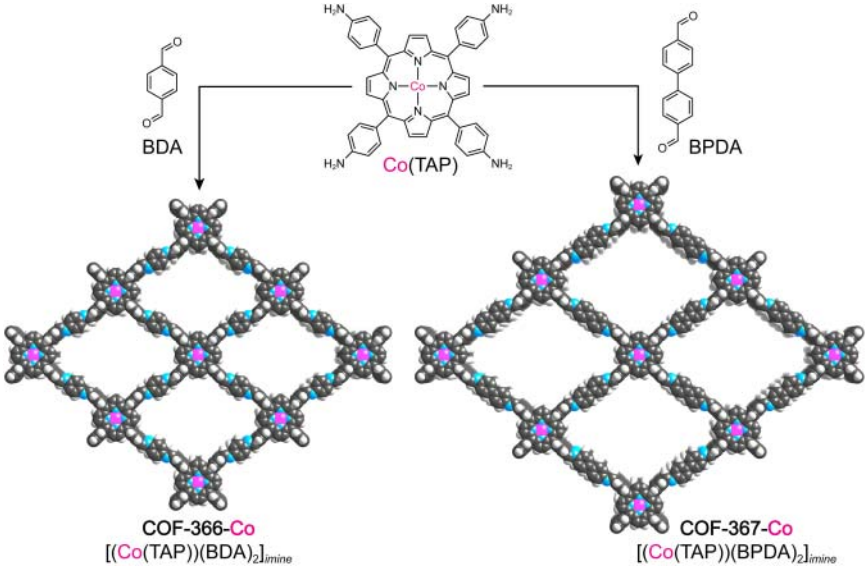

Figure 10.2 Pre-synthetic installation of Co^{2+} metal centers in COF-366 and COF-367 by metalation of the porphyrin starting material M(TAP) (M = Co^{2+}, Cu^{2+}). The cobalt-metalated COFs termed COF-366-Co and COF-367-Co are built from pre-synthetically metalated H_2TAP building units and Co^{2+} (Co(TAP)). The metal centers in these frameworks serve as active sites for the electrocatalytic conversion of CO_2 to CO. Color code: Co, pink; H, white; C, gray; N, blue.

porphyrins are active electrochemical CO_2 reduction catalysts [5]. Similarly to discrete porphyrin catalysts, COF-366-Co can electrocatalytically convert CO_2 to CO but the permanent interface of the framework with the electrode significantly enhances the performance of the material as compared to the molecular analog. An even higher performance is observed in the isoreticular expanded version, termed COF-367-Co $[(Co(TAP))(BPDA)_2]_{imine}$, constructed by reticulating the Co(TAP) with the linear ditopic BPDA (Figure 10.2).

In general, the metalation of COFs is not restricted to one single kind of metal and a series of isoreticular frameworks is accessible when the Co(TAP) building units in the synthesis are entirely or partially replaced with Cu(TAP) [6].

10.3.2 Pre-Synthetic Covalent Functionalization

COF-366-Co can be further modified covalently by making use of the framework backbone. Analogous to the optimization of molecular transition metal catalysts

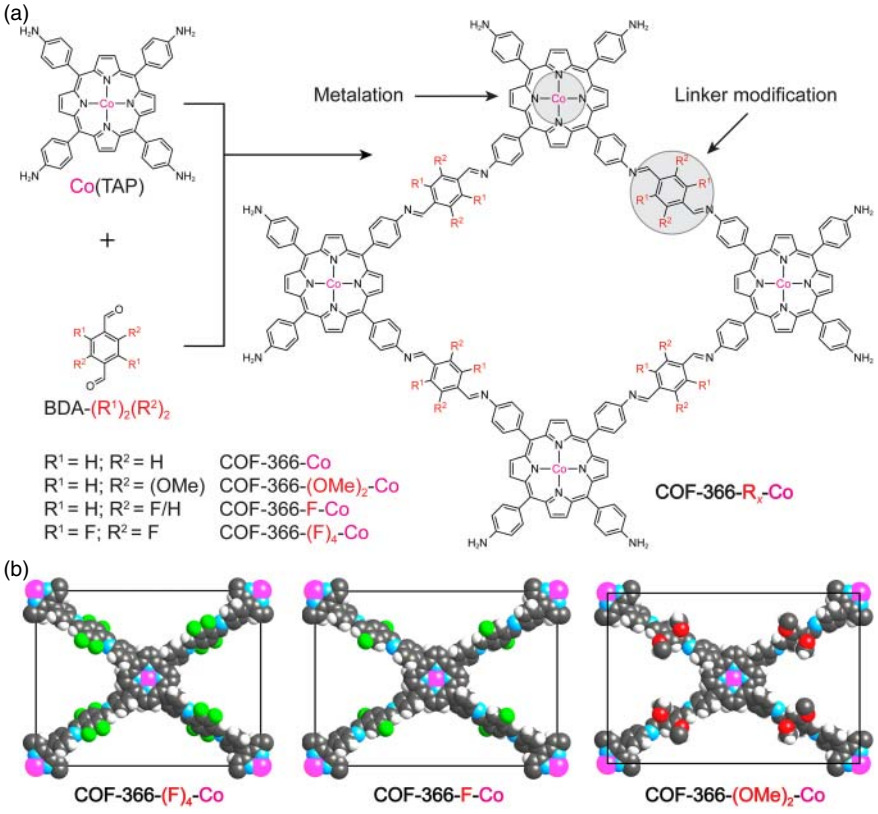

Figure 10.3 Reticular tuning of the pre-synthetically incorporated Co^{2+} active sites in a series of COF-366-Co analogs by modification of the parent structure through covalent pre-synthetic modification of the linker. (a) Substitution of the parent BDA linker with BDA-$(OMe)_2$, BDA-(F), and BDA-$(F)_4$ results in isostructural frameworks termed COF-366-Co, COF-366-$(OMe)_2$-Co, COF-366-(F)-Co, and COF-366-$(F)_4$-Co. (b) The unit cells of these COFs highlight that the underlying structure and the metrics of the substituted frameworks remain unaltered. Color code: Co, pink; H, white; C, gray; N, blue; F, green.

by modification of their ligands, COF catalysts can be optimized by covalent modification of their backbone. Inductive effects on the metal center in the cobalt porphyrins affect their catalytic performance [7]. Substitution of the BDA linker in COF-366-Co by BDA-$(F)_4$ (2,3,5,6-tetrafluoroterephthaldehyde), BDA-(F) (2-fluoroterephthaldehyde), and BDA-$(OMe)_2$ (2,5-dimethoxyterephthaldehyde) yields three functionalized COFs termed COF-366-$(F)_4$-Co, COF-366-(F)-Co, and COF-366-$(OMe)_2$-Co, respectively (Figure 10.3). The frameworks show substantial differences in reactivity as a consequence of changes in the electronic structure imparted by the pre-synthetically modified linkers, corroborating the importance of covalent functionalization of the organic linkers for the reticular tuning of COFs for specific applications [8].

10.4 Post-Synthetic Modification

In many cases functional groups interfere with the COF synthesis conditions, and consequently these functionalities need to be introduced post-synthetically. There are different means to achieve this: (i) the interior of COFs can serve as a host for the trapping of functional molecules, biomacromolecules, or nanoparticles, (ii) organic transformations can be performed on the organic backbone of the framework to append functional groups in specific positions, (iii) metal ions can be incorporated into predesigned metal coordination sites within the structure, (iv) linkers can be exchanged post-synthetically with full retention of crystallinity and definitiveness of structure, and (v) the linkage in the parent COF can be modified to alter the inherent physical and chemical properties of the framework. In the following sections we will highlight examples for these different types of post-synthetic modification.

10.4.1 Post-Synthetic Trapping of Guests

A versatile strategy to impart functionality into COFs is to make use of their large accessible pores to trap guest molecules. This is a potent mode of modification as it allows for a large variety of functional organic and inorganic molecules, biomacromolecules, or metal nanoparticles to be incorporated. In contrast to embedding of species in the pores, the incorporated guests introduced according to this principle are not limited by the need for compatibility with the COF forming reaction conditions.

10.4.1.1 Trapping of Functional Small Molecules

$[(TAPB)_2(BDA\text{-}(OMe)_2)_3]_{imine}$, a mesoporous framework constructed from trigonal tritopic TAPB and linear ditopic BDA-$(OMe)_2$, serves as a platform for solid-state proton conductors [9]. The framework crystallizes in the hexagonal space group *P*6 and features mesoporous hexagonal channels of 3.3 nm in width running along the crystallographic *c*-axis. The framework is capable of trapping large amounts of *N*-heterocyclic proton carriers such as triazole (180 wt%) and imidazole (164 wt%) inside of its mesopores (Figure 10.4). While the parent COF shows a negligible proton conductivity of 10^{-12} S cm^{-1}, the

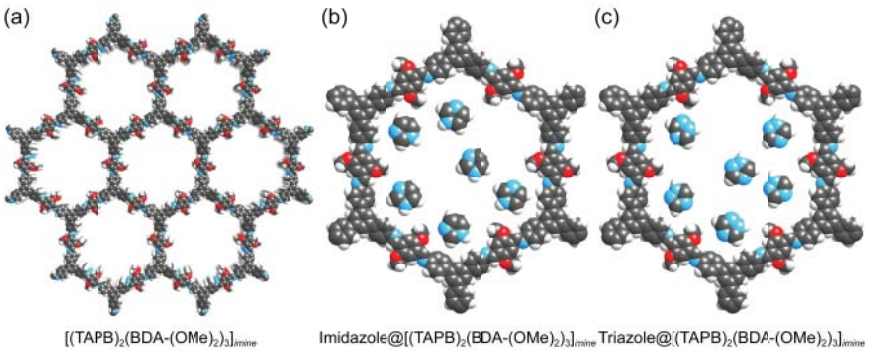

Figure 10.4 Trapping of *N*-heterocycles in the 3.3-nm-wide mesopores of the (a) imine-linked $[(TAPB)_2(BDA\text{-}(OMe)_2)_3]_{imine}$. (b) Impregnation of the material with imidazole (164 wt%) and (c) triazole (180 wt%) yields the solid-state proton conductors imidazole@$[(TAPB)_2(BDA\text{-}(OMe)_2)_3]_{imine}$ and triazole@$[(TAPB)_2(BDA\text{-}(OMe)_2)_3]_{imine}$ with conductivities of 4.37×10^{-3} S cm^{-1} and 1.1×10^{-3} S cm^{-1}, respectively. Color code: H, white; C, gray; N, blue; O, red.

triazole- and imidazole-loaded frameworks feature an increased proton conductivity (at 130 °C) of 1.1×10^{-3} S cm^{-1} and 4.37×10^{-3} S cm^{-1}, respectively. The materials retain 99.3% of the *N*-heterocyclic proton carriers under 100% relative humidity for more than 15 days [10].

10.4.1.2 Post-Synthetic Trapping of Biomacromolecules and Drug Molecules

Trypsin, a globular protein with hydrodynamic radius of 3.8 nm, can be trapped inside a COF constructed from trigonal tritopic TAPB and linear ditopic BDA-$(OH)_2$ (2,5-dihydroxyterephthalaldehyde), termed $[(TAPB)_2(BDA\text{-}(OH)_2)_3]_{imine}$ [9b]. The framework crystallizes in the hexagonal space group *P*6 and has an **hcb** topology. It features large hexagonal channels with a pore-size distribution derived from the nitrogen isotherm centered around 3.7 nm and a high surface area of 1500 m^2 g^{-1}. The hydrogen bonding in this COF endows the framework with chemical stability making it a suitable platform for protein adsorption from water. While the average pore size of the COF is marginally smaller than the hydrodynamic radius of Trypsin, this does not affect the adsorption of this biomacromolecule because soft molecules such as enzymes can adjust their conformation to fit inside the pores. The maximum storage capacity of Trypsin for this COF is 15.5 mmol g^{-1} and the loaded samples retain about 60% of the activity of the free enzyme. $[(TAPB)_2(BDA\text{-}(OMe)_2)_3]_{imine}$ can furthermore be employed for loading and release of the anticancer drug doxorubicin (DOX). The DOX loading capacity of $[(TAPB)_2(BDA\text{-}(OMe)_2)_3]_{imine}$ is 0.35 mg g^{-1} and the drug shows a slow release profile with a 42% decrease over the course of seven days in a pH 5 phosphate buffer [11].

10.4.1.3 Post-Synthetic Trapping of Metal Nanoparticles

A 3D framework formed by self-condensation of tetrahedral tetratopic TBPM termed COF-102 ($[TBPM]_{boroxine}$) is constructed from trigonal

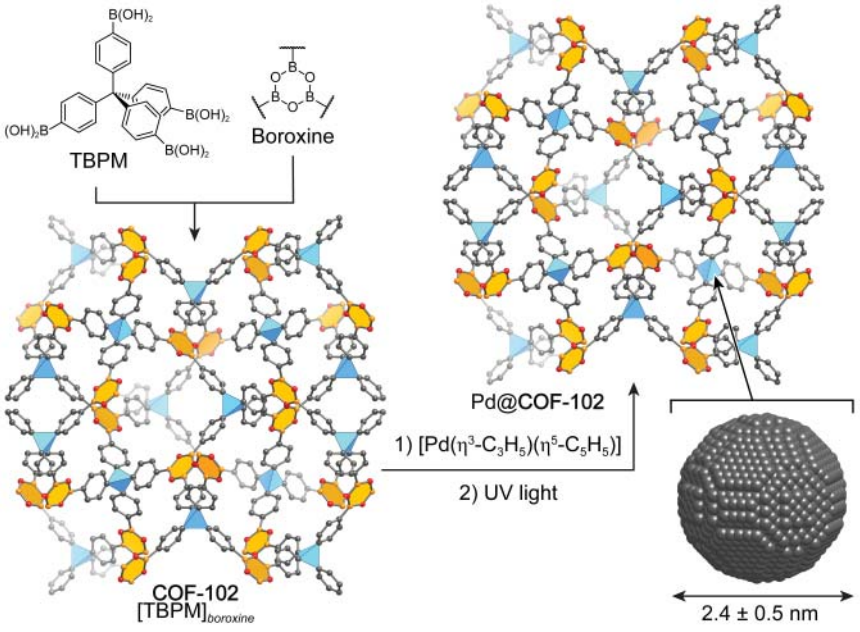

Figure 10.5 Trapping of palladium nanoparticles in the pores of the 3D boronate ester COF-102 by a precursor chemical infiltration technique. COF-102 is constructed from the self-condensation of tetrahedral tetratopic TBPM through the formation of trigonal tritopic boroxine linkages. By infiltration of the pores with the $Pd(\eta^3\text{-}C_3H_3)(\eta^5\text{-}C_5H_5)$ precursor and subsequent exposure to UV light, palladium nanoparticles are formed in the interconnected pores of the **ctn** topology framework, termed Pd@COF-102. All hydrogen atoms are omitted for clarity. Central tetrahedral carbon, blue tetrahedra; boroxine linkage, orange polygons. Color code: C, gray; N, blue; B, orange; O, red.

tritopic boroxine linkages to give a framework of **ctn** topology (Figure 10.5). Palladium nanoparticles can be trapped in the interconnected pores of COF-102 by a precursor chemical infiltration technique. The framework crystallizes in the cubic space group $I\bar{4}3d$ and features 0.9-nm-wide pores that are connected by face-sharing 1-nm-wide pore openings. Diffusion of the volatile and light-sensitive $Pd(\eta^3\text{-}C_3H_5)(\eta^5\text{-}C_5H_5)$ complex in the dark followed by irradiation with UV light results in the formation of Pd@COF-102 (Figure 10.5). TEM shows the formation of the metal-nanoparticle-loaded COF with particles of narrow size distribution centered around 2.5 nm, even at high loadings of up to 30 wt%. Notably, this size is larger than the cavity size of the pores in COF-102 of 0.9 nm, which is rationalized by the fact that the pores are interconnected thus allowing for the formation of larger, interconnected particles. Samples loaded with 9.5 wt% of palladium nanoparticles show a two- to threefold enhancement of the H_2 storage capacity of COF-102 at room temperature and 20 bar. The hydrogen uptake is reversible but cannot exclusively be rationalized by the formation of palladium hydride [12].

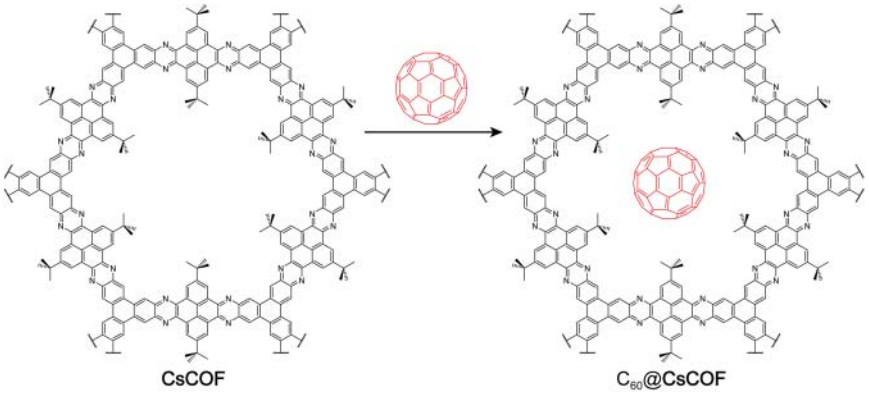

Figure 10.6 Trapping of fullerene C_{60} in the highly conjugated phenazine-linked CsCOF. The pore size of the framework allows for exactly one molecule of C_{60} per cross-section of each pore. The C_{60}@CsCOF construct serves as an active layer for efficient photoenergy conversion and shows a power conversion efficiency of 0.9% and an open-circuit voltage of 0.98 V.

10.4.1.4 Post-Synthetic Trapping of Fullerenes

CS-COF is a framework constructed from trigonal tritopic HATP (2,3,6,7,10,11-hexaminotriphenylene) and linear ditopic PTO (2,7-di-*tert*-butylpyrene-4,5,9,10-tetraone) through phenazine bond formation (Figure 10.6) [13]. The highly conjugated framework is a high rate hole-conducting framework with an exceptional mobility of 4.2 $cm^2\ V^{-1}\ s^{-1}$. By impregnation with fullerene molecules with a loading of 25 wt% an ordered bi-continuous donor–acceptor system termed C_{60}@CS-COF is obtained. Owing to the offset stacking of the COF layers as well as the presence of bulky *tert*-butyl groups on the linker pointing into the channels, the pore size of CS-COF is reduced to about 1.6 nm resulting in the presence of exactly one C_{60} molecule in the cross-section of each pore (Figure 10.6). C_{60}@CS-COF can serve as the active layer for photoenergy conversion and shows a power conversion efficiency of 0.9% with a large open-circuit voltage of 0.98 V upon irradiation.

10.4.2 Post-Synthetic Metalation

Post-synthetic metalation of COFs is utilized to incorporate transition-metal complexes into COFs that cannot be incorporated pre-synthetically. The metal coordination site can either be the linkage itself which forms *in situ* and thus cannot be metalated pre-synthetically, or it can be a binding site on the linker that does not withstand the COF forming reactions. Here, we provide examples for both scenarios.

10.4.2.1 Post-Synthetic Metalation of the Linkage

Imine type ligands are versatile binding motifs in coordination chemistry. This is exploited in COF chemistry for the metalation of imine-linked frameworks as exemplified by the **hcb** topology COF LZU-1 ($[(TFB)_2(PDA)_3]_{imine}$) (Figure 10.7a) [14]. LZU-1 is built from trigonal tritopic TFB and linear ditopic

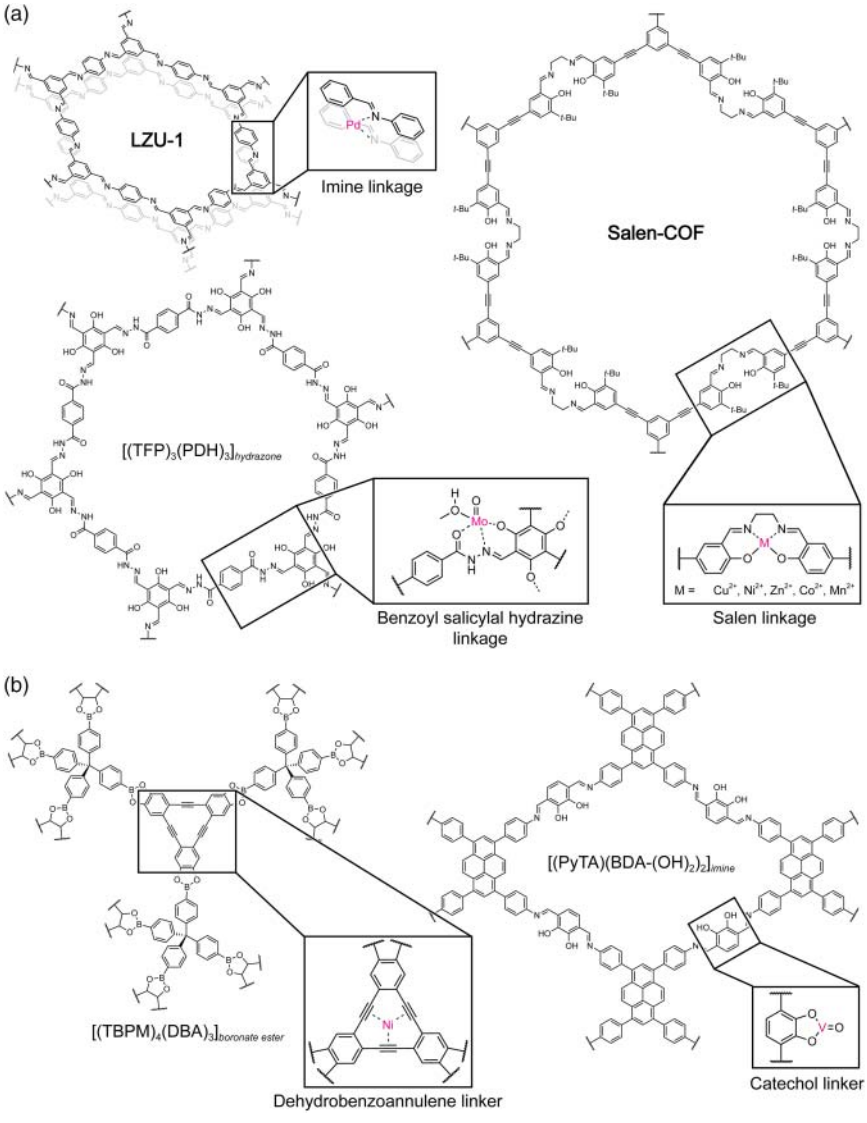

Figure 10.7 Post-synthetic metalation is carried out to introduce metal ions into COFs when they cannot be incorporated pre-synthetically due to limitations with respect to complex stability or because the binding sites are generated during the reticulation process. (a) Linkages of COFs can serve as metal coordination sites as in the case of Salen linkages in Salen-COF, benzoyl salicylal hydrazine linkages in $[(TFP)_2(PDH)_3]_{hydrazone}$, or the imine linkages in LZU-1. (b) Metalation sites can also be introduced into the frameworks as linkers. Examples for such coordination sites are dehydrobenzannulene units in $[(TBPM)_3(DBA)_4]_{boronate\ ester}$ or catechol moieties in $[(PyTA)(BDA\text{-}(OH)_2)_2]_{imine}$.

PDA. The framework crystallizes in the hexagonal space group *P*6/*m* and features 1.8-nm-wide channels running along the crystallographic *c*-axis. The distance between the imine groups of adjacent layers is 3.7 nm, which constitutes the ideal distance for binding of a metal ion to two imine bonds of neighboring COF layers. Treatment of LZU-1 with a solution of a $Pd(OAc)_2$ results in the formation of the corresponding metalated COF termed LZU-1-Pd. Changes in the binding energy of Pd^{2+} by 0.7 eV from 338.4 eV for the free $Pd(OAc)_2$ to 337.7 eV for LZU-1-Pd are observed by X-ray photoelectron spectroscopy, thus confirming the binding of the metal species to the framework. Molecular palladium complexes are known catalysts for cross-coupling reactions but their homogeneous nature complicates catalyst recycling [15]. LZU-1 catalyzes Suzuki–Miyaura cross-coupling reactions with a broad substrate scope and excellent yields of conversion (96–98%). The high stability and recyclability of the COF catalyst renders this approach promising for the heterogenization of molecular catalysts (Figure 10.7a).

The molybdenum-functionalized framework $[(TFP)_2(PDH)_3]_{hydrazone}$ is synthesized by reticulation of trigonal tritopic TFP with linear ditopic PDH (1,4-dicarbonyl-phenyl-dihydrazide). The linkages of this hydrazone-linked COF are benzoyl salicylal hydrazine ligands, which can coordinate to $MoO_2(acac)_2$ (acac = acetylacetonate). The introduction of the molybdenum species into the framework is achieved by immersing the COF in a methanol solution of $MoO_2(acac)_2$ resulting in an efficient organomolybdenum catalyst with a high active site density of 2.0 mmol g^{-1}. The binding of the COF to molybdenum is confirmed by XPS studies, which indicate the strong coordination of Mo^{2+} to the benzoyl salicylic hydrazine groups of $[(TFP)_2(PDH)_3]_{hydrazone}$. The metalated COF shows high catalytic activity for the epoxidation of cyclohexene with conversion above 99%. Recovery of the catalyst is achieved by filtration and the COF can be reused for more than four cycles with retention of the catalytic activity (Figure 10.7a) [16].

10.4.2.2 Post-Synthetic Metalation of the Linker

A metal-binding motif that is introduced as a linker is found in a framework constructed from tetratopic PyTA (4,4′,4″,4‴(pyrene-1,3,6,8-tetrayl)tetraaniline) and linear ditopic BDA-$(OH)_2$ building units, termed $[(PyTA)(BDA\text{-}(OH)_2)_2]_{imine}$ (Figure 10.7b) [17]. In this structure, the catechol moieties of the BDA-$(OH)_2$ linkers point into the 2.4-nm-wide trapezoidal channels running along the crystallographic *c*-axis of this **sql** topology framework. Treatment of these catechol groups with vanadium(IV)-oxy acetylacetonate results in the formation of V=O moieties bound to the catechol binding sites with near-quantitative conversion (0.96 V=O moieties per catechol unit).

Dehydrobenzoannulene macrocycles are known to coordinate to a number of different metal species [18]. The binding of metal ions in such organometallic complexes is weak and thus this binding motif can only be realized in COFs through post-synthetic metalation pathways. The **ctn** topology framework $[(TBPM)_3(DBA)_4]_{boronate\ ester}$ (where DBA = hexahydroxydehydrobenzoannulene) is constructed from tetrahedral tetratopic TBPM and trigonal tritopic DBA through boronate ester bond formation (Figure 10.7b) [19]. The high porosity of the framework is highlighted by its large BET surface

area of 5083 m^2 g^{-1}. Metalation of the dehydrobenzoannulene core of the DBA linkers with $Ni(COD)_2$ (COD = 1,5-cyclooctadiene) yields the metalated ($[(TBPM)_3(DBA)_4]_{boronate\ ester}$)-Ni. Only a small decrease in the gravimetric surface area is observed upon metalation (4763 m^2 g^{-1}), attributable to the increase in framework density. Comparison of the UV–vis diffuse-reflectance spectra of $[(TBPM)_3(DBA)_4]_{boronate\ ester}$ and ($[(TBPM)_3(DBA)_4]_{boronate\ ester}$)-Ni show that the parent material exhibits a broad absorbance between 300 and 420 nm whereas in the metalated analog a new absorption band centered around 575 nm is observed, analogous to what is observed in the discrete DBA–Ni^0 complex. The introduced Ni^0 centers impart ($[(TBPM)_3(DBA)_4]_{boronate\ ester}$)-Ni with luminescent properties with λ_{max}, the wavelength of highest intensity, located at 510 nm.

10.4.3 Post-Synthetic Covalent Functionalization

Covalent post-synthetic modification of the linker is performed to introduce functional groups into the framework that would interfere with the COF forming reaction. This interference can either be due to the functional group reacting with the building units that form the framework (e.g. amines in the synthesis of imine linked COFs) or because the functionality manipulates the COF forming equilibrium (e.g. carboxylic acids in the formation of imine COFs). To introduce these functionalities post-synthetically, reactions need to be chosen that occur with high yields and under conditions that ensure that the integrity of the framework is retained. In COF chemistry, covalent modification is often achieved by copper(I)-catalyzed click reactions, and either alkynes or azides can be anchored to the COF backbone pre-synthetically to serve as sites of modification (Figure 10.8a). A large variety of functional groups such as alkyls, hydroxyls, esters, anhydrides, or amines can be incorporated into COFs according to this approach. Other reactions that are commonly employed in COF chemistry are succinic anhydride ring-opening reactions to form carboxylic acids, nitro reductions to introduce amines, or aminolysis to yield amides (Figure 10.8b,c).

10.4.3.1 Post-Synthetic Click Reactions

COFs bearing highly functionalized backbones are difficult to obtain by means of pre-synthetic functionalization of their constituents since for each additional appended functionality synthetic conditions need to be identified to crystallize the COF. Additionally, the functional group tolerance of the solvothermal COF synthesis conditions restricts what type of functionalities can be incorporated in this way. One strategy to introduce a wide array of functional groups post-synthetically is based on copper(I)-catalyzed click reactions, which occur under mild reaction conditions and are orthogonal to a lot of chemical functionalities. COFs incorporating alkynyl-functionalized building units can serve as platforms for covalent post-synthetic functionalization using this protocol. Reactions of BDA-(H_2C—C≡CH) (2,5-bis(2-propynyloxy)terephthalaldehyde) and BDA-$(OMe)_2$ at different molar ratios with H_2(TAP) yield an **sql** topology framework termed COF-366-(X%[H_2C—C≡CH]) (X = 0–100) with different amounts of ethynyl groups pointing into the 1.8-nm-wide square-shaped channels of

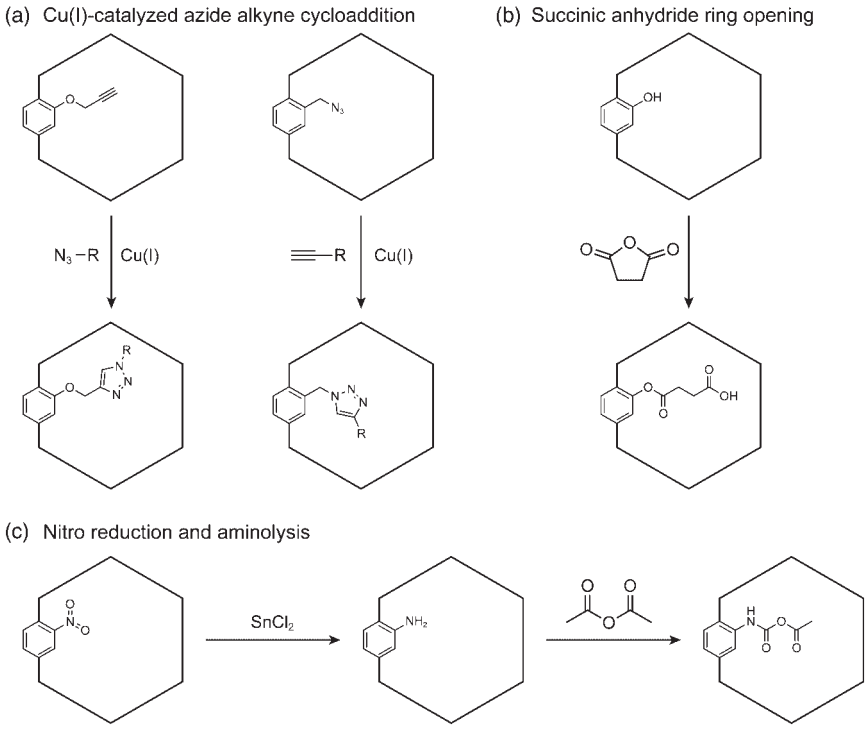

Figure 10.8 Covalent post-synthetic modification reactions employed in COFs. (a) Reaction of alkynes on the COF backbone with organic azides are performed by copper(I)-catalyzed click reactions. Similarly, the COF backbone can be functionalized with organic azides that are reacted with alkynes to yield triazole derivatives. (b) COFs bearing hydroxyl groups are reacted with succinic anhydride to yield frameworks containing carboxylic acid functionalities. (c) Nitro groups in the framework are reduced by $SnCl_2$ to yield COFs with amino groups. In a second step, aminolysis of amino functionalities yields amide-grafted COFs.

the framework (Figure 10.9). Post-synthetic click reactions are employed to introduce the stable organic radical TEMPO (4-azido-2,2,6,6-tetramethyl-1-piperidinyloxy) to yield the corresponding functionalized framework (Figure 10.9). Owing to the large number of accessible radicals of the TEMPO substituents in the functionalized framework, the COF can undergo rapid and reversible redox reactions, leading to capacitive energy storage with high capacitance, high-rate kinetics, and robust cycle stability (Figure 10.9) [20].

Similarly, quantitative click reactions between the ethynyl units on the COF-366-(X%[H_2C—C≡CH]) backbone and azide compounds can be performed to anchor ethyl, acetate, hydroxyl, carboxylic acids, and amino groups. Investigation of the CO_2 uptake capacities of such COFs shows that the functionalization has a profound impact on the sorption behavior. The material functionalized with 50% of amino substituents shows the highest uptake capacity of 157 mg g^{-1}, thus illustrating the utility of post-synthetic covalent modifications for performance screening of a large number of framework structures (Figure 10.9) [21].

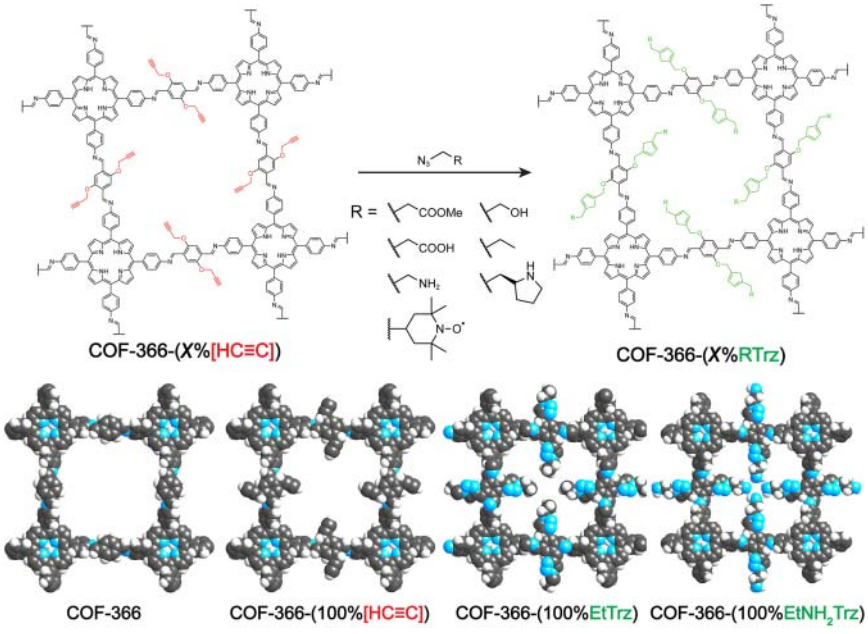

Figure 10.9 Covalent modification of the imine-linked COF-366 by copper(I)-catalyzed click chemistry. A variety of functional groups including TEMPO, ethyl, ester, hydroxyl, acetic anhydride, and primary amine moieties are introduced into the channels of the pre-synthetically functionalized framework COF-366-(*X*%[H_2C—C≡CH]) bearing various amounts of alkyne functionalities. The parent COF-366, the pre-synthetically functionalized COF-366-(100%[H_2C—C≡CH]), and post-synthetically functionalized COF-366-(100%EtTrz) (Trz = triazine) and COF-366-(100%EtNH_2Trz) are illustrated as examples. Color code: H, white; C, black; N, blue.

COFs with chiral substituents can be created by introducing (*S*)-pyrrolidine into the backbone of COF-366-(*X*%[H_2C—C≡CH]) (*X* = 25%, 50%, 75%, and 100%). Subjecting these frameworks to post-synthetic modification yields COFs functionalized with different amounts of (*S*)-pyrrolidine (Figure 10.9). The frameworks show catalytic activity for enantioselective Michael-addition reactions. Benchmarking against the molecular (*S*)-4-(phenoxymethyl)-1-(pyrrolidin-2-ylmethyl)-1*H*-1*H*-1,2,3-triazole catalyst shows that the molecular catalyst requires 3.3 hours for completion and catalyzes the reaction with an enantiomeric excess of 49%. In contrast, the COF catalysts achieve similar enantiomeric excess (44–51%) but the framework functionalized at 25% completes the reaction in just one hour, thus outperforming not only the molecular model catalyst but also the other COF catalysts with higher catalyst loading. This highlights the necessity for the optimization of the interplay between pore aperture and the amount of exposed functional groups on the rate of the catalytic transformations [22].

Owing to the benign reaction conditions, click chemistry as a tool for covalent post-synthetic modification is not limited to imine COFs but can also be applied to the functionalization of boronate ester COFs. Many substituents interfere in boronate ester COF formation due to their inherent low hydrolytic

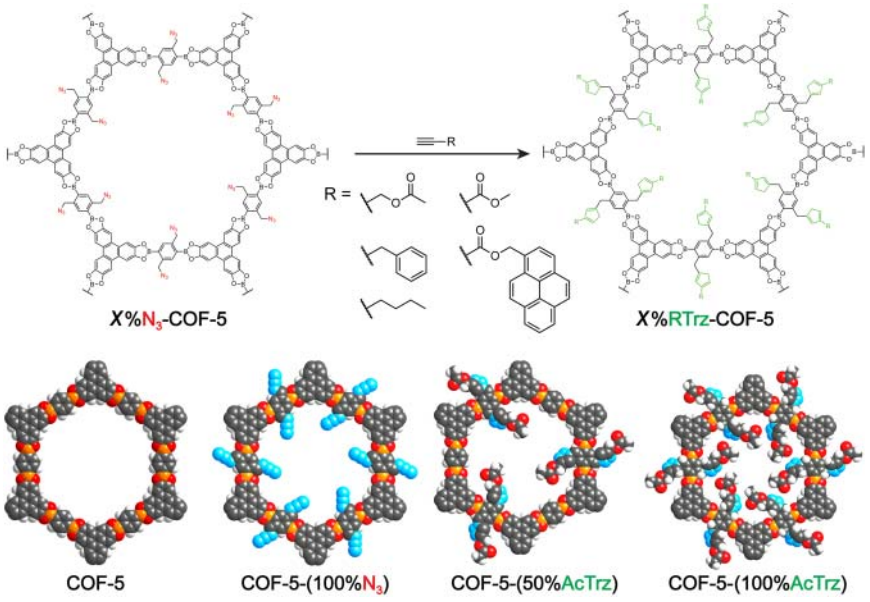

Figure 10.10 Covalent modification of the boronate ester linked COF-5 by copper(I)-catalyzed click chemistry. A variety of functional groups including acetate, butyl, phenyl, ester, and pyrene moieties can be introduced into the channels of pre-synthesized COF-5-*X*%N_3 bearing different amounts of azide functionalities by means of copper-catalyzed click reactions. This covalent functionalization of the framework occurs without compromising the fidelity and crystallinity of the underlying structure. The parent COF-5 structure, COF-5-(100%N_3), COF-5-(50%AcTrz), and COF-5-(100%AcTrz) are illustrated as examples. Color code: H, white; C, gray; N, blue; B, orange; O, red.

stability. As such, post-synthetic covalent modification is utilized to impart these frameworks with functionality. In the case of the pre-synthetic functionalization of COF-5, the framework is reticulated from HHTP with varying ratios of BDBA (1,4-phenylene diboronic acid) and its azide functionalized analog BDBA-(H_2C–N_3) (Figure 10.10). Here, the post-synthetic functionalization of the framework is achieved by reacting the predisposed azide functionalities with functionalized alkynes, again by copper(I)-catalyzed click chemistry. Various functional groups such as acetyl, butyl, phenyl, methyl esters, or pyrene moieties can be appended with full retention of the crystallinity of the parent structure [23].

10.4.3.2 Post-Synthetic Succinic Anhydride Ring Opening

A different strategy is applied for the introduction of carboxylic acid groups. Carboxylic acids interfere with the formation of Schiff-base COFs since they act as catalysts for imine formation and as such disturb the reaction equilibrium. To introduce carboxylic acids post-synthetically the use of ring-opening reactions of phenolic units on the linker with succinic anhydride are employed. The feasibility of this approach is once again demonstrated for COF-366, in this case formed from H_2TAP and varying ratios of BDA and BDA-$(OH)_2$ (Figure 10.11).

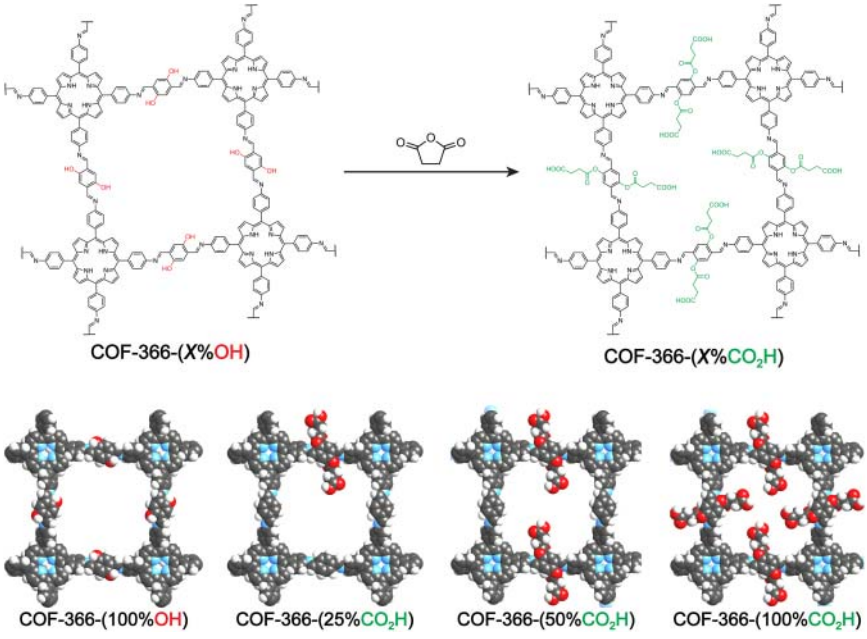

Figure 10.11 Post-synthetic succinic anhydride ring-opening reaction on COF-366-(X%OH). Hydroxyl groups are introduced into the parent COF-366 structure by substituting (partially or completely) BDA with BDA-(OH) during the synthesis. Pre-synthetically functionalized COF-366-(100%OH) and post-synthetically modified COF-366-(25%CO_2H), COF-366-(50%CO_2H), and COF-366-(100%CO_2H) are shown as examples for this approach. Color code: H, white; C, gray; N, blue; O, red.

Frameworks with varying amounts of hydroxyl groups and their carboxyl group functionalized derivatives differ significantly with respect to their CO_2 sorption behavior. The binding affinity of the framework for CO_2 correlates with the nature and amount of the functional groups present in the pores. The framework with 100% carboxylic acid functionalities shows the highest binding affinity with a Q_{st} value of $-43.5\,kJ\,mol^{-1}$ that far exceeds the value for the hydroxyl group functionalized progenitor of $-36.4\,kJ\,mol^{-1}$. Notably, compared to click chemistry this type of reaction requires no metal catalysts and proceeds cleanly, representing a promising strategy for covalent post-synthetic modification [21].

10.4.3.3 Post-Synthetic Nitro Reduction and Aminolysis

The post-synthetic introduction of amides into COFs can be achieved by means of a two-step post-synthetic modification. The **hcb** topology framework $[(TFP)_2(BZ\text{-}(NO_2)_3]_{\beta\text{-}ketoenamine}$ is constructed from trigonal tritopic TFP and linear ditopic BZ-$(NO_2)_2$ (2,2′-dinitrobenzidine) through β-ketoenamine bond formation (Figure 10.12) [24]. Amines on the linker would interfere with the reticulation as they react with the TFP building units, and therefore a post-synthetic approach needs to be employed. In the first step, the nitro groups on the as-synthesized COF are reduced by $SnCl_2$ to afford the amine functionalized framework, termed $[(TFP)_2(BZD\text{-}(NH_2)_3]_{\beta\text{-}ketoenamine}$. The resulting

Figure 10.12 Two-step post-synthetic conversion of nitro groups in the mesoporous $[(TFP)_2(BZ\text{-}(NO_2)_3]_{\beta\text{-}ketoenamine}$: reduction of the preinstalled nitro groups on the linker to amines using $SnCl_2$ followed by aminolysis of acetic anhydride yield the amide functionalized $[(TFP)_2(BZ\text{-}((NHCOCH_3)_2)_3]_{\beta\text{-}ketoenamine}$. Owing to the high inherent chemical stability of the frameworks' β-ketoenamine linkages and the basic character of the introduced functionalities the resulting materials are utilized for vapor sorption of lactic acid. Color code: H, white; C, gray; N, blue; O, red.

framework can now make use of the amine moieties on the linker and this is illustrated by aminolysis of acetic anhydride as the second step to obtain the amide functionalized COF, termed $[(TFP)_2(BZ\text{-}((NHCOCH_3)_2)_3]_{\beta\text{-}ketoenamine}$ (Figure 10.12). Owing to the acid stability of these frameworks endowed by the β-ketoenamine linkages and the basic character of the introduced functionalities they are employed as a sorbent for lactic acid. Comparison of $[(TFP)_2(BZ\text{-}(NO_2)_3]_{\beta\text{-}ketoenamine}$, and $[(TFP)_2(BZ\text{-}((NHCOCH_3)_2)_3]_{\beta\text{-}ketoenamine}$ reveals that the amine-functionalized material has the highest uptake (6.6 wt%), followed by the amide-functionalized analog (4.0 wt%), whereas the parent framework only shows an uptake of 2.5 wt%.

10.4.3.4 Post-Synthetic Linker Exchange

Construction of an imine-linked COF from tetratopic TCA ((1,1′,3′,1″-terphenyl)-3,3″,5,5″-tetracarbaldehyde) and linear ditopic BZ building units yields $[(TCA)(BZ)_2]_{imine}$. This framework crystallizes in the hexagonal space group *P*6 and in an unusual **fxt** net. The framework has three distinct kinds of pore. One micropore that is not gas accessible and two different mesopores with the maxima in the pore-size distribution centered around 2.56 and 3.91 nm. The BZ linkers in this framework can be exchanged to shorter PDA linkers without losing the crystallinity of the framework. Owing to the increased electron density on the two nitrogen atoms introduced by the inductive effect of the respective electron donating amine functionality in the para-positions, the amines of the shorter PDA linker are more nucleophilic than the ones in BZ. Hence, under reversible conditions the linkers exchange, resulting in the formation of an isoreticular analog of the framework with decreased pore size (Figure 10.13). Exposing $[(TCA)(BZ)_2]_{imine}$ to PDA in the presence of acetic acid as a catalyst yields a new COF termed $[(TCA)(PDA)_2]_{imine}$ over the course of just four hours. The expected change in unit cell dimensions is confirmed by PXRD and the position of the respective maxima in the pore-size distribution shift to smaller

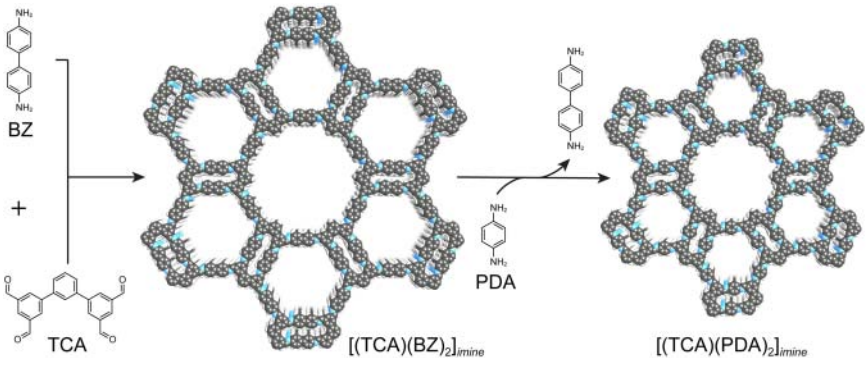

Figure 10.13 An isoreticular analog of the **fxt** topology framework $[(TCA)(BZ)_2]_{imine}$ is obtained by post-synthetic linker exchange of the frameworks' BZ linkers with the shorter PDA. The resulting framework, termed $[(TCA)(PDA)_2]_{imine}$ retains the overall topology and symmetry of its progenitor but features smaller pore sizes. Color code: H, white, C, gray; N, blue.

values of 1.61 and 3.18 nm, in good agreement with the proposed structural model [24].

10.4.3.5 Post-Synthetic Linkage Conversion

Many physico-chemical properties of COFs are determined by the linkage that is used to reticulate the building units into an extended framework structure. Consequently, a lot of research efforts have been devoted to devising new linkage chemistries [25]. For every new linkage a new set of conditions needs to be identified under which the reaction occurs with microscopic reversibility to allow for error correction and thus the formation of the material without defects and in crystalline form. This severely limits the number of suitable linkages in COF chemistry, as many reactions are difficult to run under thermodynamic control and we have covered this challenge in Chapter 8. A strategy to circumvent this very issue is to post-synthetically convert linkages within the crystallized COF. This is illustrated by the conversion of the two COFs, $[(TAPB)_2(BDA)_3]_{imine}$ and $[(ETTA)(BDA)_2]_{imine}$ (where ETTA = 1,1,2,2-tetrakis(4-aminophenyl)ethane), from their imine progenitors to the respective amide-linked counterparts. $[(TAPB)_2(BDA)_3]_{imine}$ is formed from trigonal tritopic TAPB by reticulation with linear ditopic BDA. The resulting framework crystallizes in the hexagonal space group *P*6 and has an underlying **hcb** topology (Figure 10.14). In contrast, $[(ETTA)(BDA)_2]_{imine}$ is constructed from tetratopic ETTA (1,1,2,2-tetrakis(4-aminophenyl)ethane) and BDA building units and has an underlying **kgm** net. Both frameworks feature wide mesoporous hexagonal channels along the crystallographic *c*-direction and therefore allow for facile access of reagents to the sites of conversion throughout the entire material. The conversion of the two frameworks to their amide-linked counterparts is effected by a Pinnick-style oxidation in a mixture of dioxane, acetic acid, and $NaOCl_2$ as an oxidant in the presence of 2-methyl-2-butene as a proton scavenger. The oxidation occurs at room temperature over the course of two days. The resulting amidated frameworks termed $[(TAPB)_2(BDA)_3]_{amide}$

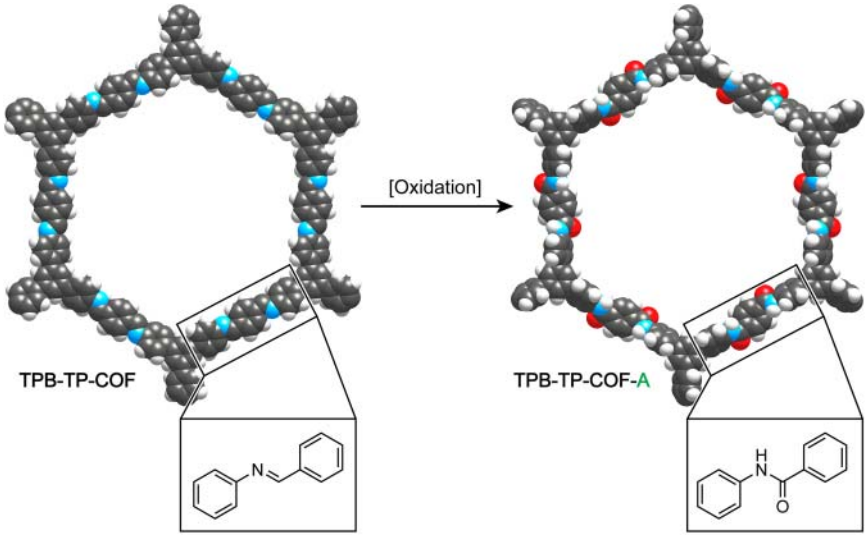

Figure 10.14 Post-synthetic linkage modification of $[(TAPB)_2(BDA)_3]_{imine}$ by oxidation of the imine linkages to chemically more inert amide bonds. The symmetry and structure metrics of the parent framework are retained in the resulting $[(TAPB)_2(BDA)_3]_{amide}$. The modified framework shows a significantly improved chemical stability toward acid and base. Color code: H, white; C, black, N, blue; O, red.

and $[(ETTA)(BDA)_2]_{amide}$ fully retain the crystallinity of their progenitors, albeit with lower surface areas (Figure 10.14). The conversion of the frameworks is confirmed by FT-IR spectroscopy where the complete disappearance of the C=N stretch of the imine bond at ~1620 cm^{-1} and the appearance of the C=O stretch of the amide carbonyl bond at ~1655 cm^{-1} are observed. The conversion is further substantiated by isotopically enriched ^{13}C CP-MAS (^{13}C cross-polarization magic angle spinning) NMR spectra, which show a clear shift of the imine carbon in the starting material at 157 ppm upon oxidation to the amide carbonyl carbon at 166 ppm. The amide-linked COFs show improved chemical stability to both acid and base. Treatment with 12 M aqueous HCl and 1 M aqueous NaOH for 24 hours results in the amorphization and partial dissolution of the imine-linked $[(TAPB)_2(BDA)_3]_{imine}$; however, the amide-linked $[(TAPB)_2(BDA)_3]_{amide}$ fully retains its crystallinity under these conditions [26].

10.5 Summary

Functionalization of covalent organic frameworks is a powerful tool for imparting functionality onto the ordered backbone of these materials. The organic backbone of COFs can be covalently modified pre- and post-synthetically by making use of the extensive toolbox of synthetic organic chemistry and both, the building units as well as the linkage can be targeted. Similarly both, the linkages, as well as the building units can be used as binding sites for the incorporation of metal centers. The pores of COFs can trap functional molecules, biomacromolecules,

or nanoparticles. Finally, nanoparticles can be embedded within the crystallites of the extended framework *in situ*. The fact that COFs are porous is crucial for all of the aforementioned functionalization strategies as this not only provides the space for functional groups to be added to the framework without compromising the fidelity and overall metrics of the structure but also because it enables the access to these active sites. Consequently COFs can be considered a true extension of synthetic organic chemistry to the solid state. This gives rise to the notion of treating crystals as molecules. In Chapter 11 we will cover how the macroscopic and nanoscopic morphology of COFs can be structured.

References

1 Smith, B.J., Overholts, A.C., Hwang, N., and Dichtel, W.R. (2016). Insight into the crystallization of amorphous imine-linked polymer networks to 2D covalent organic frameworks. *Chemical Communications* 52 (18): 3690–3693.

2 Tan, J., Namuangruk, S., Kong, W. et al. (2016). Manipulation of amorphous-to-crystalline transformation: towards the construction of covalent organic framework hybrid microspheres with NIR photothermal conversion ability. *Angewandte Chemie International Edition* 55 (45): 13979–13984.

3 Rodríguez-San-Miguel, D., Yazdi, A., Guillerm, V. et al. (2017). Confining functional nanoparticles into colloidal imine-based COF spheres by a sequential encapsulation-crystallization method. *Chemistry - A European Journal* 23 (36): 8623–8627.

4 Wan, S., Gándara, F., Asano, A. et al. (2011). Covalent organic frameworks with high charge carrier mobility. *Chemistry of Materials* 23 (18): 4094–4097.

5 Behar, D., Dhanasekaran, T., Neta, P. et al. (1998). Cobalt porphyrin catalyzed reduction of CO_2. Radiation chemical, photochemical, and electrochemical studies. *The Journal of Physical Chemistry A* 102 (17): 2870–2877.

6 Lin, S., Diercks, C.S., Zhang, Y.-B. et al. (2015). Covalent organic frameworks comprising cobalt porphyrins for catalytic CO_2 reduction in water. *Science* 349 (6253): 1208–1213.

7 Leung, K., Nielsen, I.M., Sai, N. et al. (2010). Cobalt-porphyrin catalyzed electrochemical reduction of carbon dioxide in water. 2. Mechanism from first principles. *The Journal of Physical Chemistry A* 114 (37): 10174–10184.

8 Diercks, C.S., Lin, S., Kornienko, N. et al. (2017). Reticular electronic tuning of porphyrin active sites in covalent organic frameworks for electrocatalytic carbon dioxide reduction. *Journal of the American Chemical Society* 140 (3): 1116–1122.

9 (a) Xu, H., Gao, J., and Jiang, D. (2015). Stable, crystalline, porous, covalent organic frameworks as a platform for chiral organocatalysts. *Nature Chemistry* 7 (11): 905–912. (b) Rosa, D.P., Pereira, E.V., Vasconcelos, A.V.B. et al. (2017). Determination of structural and thermodynamic parameters of bovine α-trypsin isoform in aqueous-organic media. *International Journal of Biological Macromolecules* 101: 408–416.

10 Xu, H., Tao, S., and Jiang, D. (2016). Proton conduction in crystalline and porous covalent organic frameworks. *Nature Materials* 15: 722–726.

11 Kandambeth, S., Venkatesh, V., Shinde, D.B. et al. (2015). Self-templated chemically stable hollow spherical covalent organic framework. *Nature Communications* 6: 6786.

12 (a) Cote, A.P., Benin, A.I., Ockwig, N.W. et al. (2005). Porous, crystalline, covalent organic frameworks. *Science* 310 (5751): 1166–1170. (b) Kalidindi, S.B., Oh, H., Hirscher, M. et al. (2012). Metal@COFs: covalent organic frameworks as templates for Pd nanoparticles and hydrogen storage properties of Pd@ COF-102 hybrid material. *Chemistry - A European Journal* 18 (35): 10848–10856.

13 Guo, J., Xu, Y., Jin, S. et al. (2013). Conjugated organic framework with three-dimensionally ordered stable structure and delocalized π clouds. *Nature Communications* 4: 2736.

14 Ding, S.-Y., Gao, J., Wang, Q. et al. (2011). Construction of covalent organic framework for catalysis: Pd/COF-LZU1 in Suzuki–Miyaura coupling reaction. *Journal of the American Chemical Society* 133 (49): 19816–19822.

15 Clayden, J., Greeves, N., Warren, S., and Wothers, P. (2001). *Organic Chemistry*, 1e. Oxford: Oxford University Press.

16 Zhang, W., Jiang, P., Wang, Y. et al. (2014). Bottom-up approach to engineer a molybdenum-doped covalent-organic framework catalyst for selective oxidation reaction. *RSC Advances* 4 (93): 51544–51547.

17 Chen, X., Huang, N., Gao, J. et al. (2014). Towards covalent organic frameworks with predesignable and aligned open docking sites. *Chemical Communications* 50 (46): 6161–6163.

18 Campbell, K., McDonald, R., Ferguson, M.J., and Tykwinski, R.R. (2003). Functionalized macrocyclic ligands: big building blocks for metal coordination. *Organometallics* 22 (7): 1353–1355.

19 Baldwin, L.A., Crowe, J.W., Pyles, D.A., and McGrier, P.L. (2016). Metalation of a mesoporous three-dimensional covalent organic framework. *Journal of the American Chemical Society* 138 (46): 15134–15137.

20 Xu, F., Xu, H., Chen, X. et al. (2015). Radical covalent organic frameworks: a general strategy to immobilize open-accessible polyradicals for high-performance capacitive energy storage. *Angewandte Chemie International Edition* 54 (23): 6814–6818.

21 Huang, N., Krishna, R., and Jiang, D. (2015). Tailor-made pore surface engineering in covalent organic frameworks: systematic functionalization for performance screening. *Journal of the American Chemical Society* 137 (22): 7079–7082.

22 Xu, H., Chen, X., Gao, J. et al. (2014). Catalytic covalent organic frameworks via pore surface engineering. *Chemical Communications* 50 (11): 1292–1294.

23 Nagai, A., Guo, Z., Feng, X. et al. (2011). Pore surface engineering in covalent organic frameworks. *Nature Communications* 2: 536.

24 Lohse, M.S., Stassin, T., Naudin, G. et al. (2016). Sequential pore wall modification in a covalent organic framework for application in lactic acid adsorption. *Chemistry of Materials* 28 (2): 626–631.

25 (a) DeBlase, C.R. and Dichtel, W.R. (2016). Moving beyond boron: the emergence of new linkage chemistries in covalent organic frameworks. *Macromolecules* 49 (15): 5297–5305. (b) Waller, P.J., Gándara, F., and Yaghi, O.M. (2015). Chemistry of covalent organic frameworks. *Accounts of Chemical Research* 48 (12): 3053–3063. (c) Diercks, C.S. and Yaghi, O.M. (2017). The atom, the molecule, and the covalent organic framework. *Science* 355 (6328): eaal1585.

26 Waller, P.J., Lyle, S.J., Osborn Popp, T.M. et al. (2016). Chemical conversion of linkages in covalent organic frameworks. *Journal of the American Chemical Society* 138 (48): 15519–15522.